Biophysical Journal
Article

Biophysical Society

Parkinson's disease-associated mutations in α-synuclein alters its lipid-bound state

Sofiya Maltseva,[1,4] Daniel Kerr,[1,3,4] Miah Turke,[1,4] Erin J. Adams,[2] and Ka Yee C. Lee[1,3,4,*]
[1]Department of Chemistry, The University of Chicago, Chicago, Illinois; [2]Department of Biochemistry and Molecular Biology, The University of Chicago, Chicago, Illinois; [3]Institute for Biophysical Dynamics, The University of Chicago, Chicago, Illinois; and [4]James Franck Institute, The University of Chicago, Chicago, Illinois

ABSTRACT Lipid-binding properties of α-synuclein play a central role in protein aggregation and progression of Parkinson's disease (PD). α-Synuclein, an intrinsically disordered protein, binds to lipid membranes through the formation of two amphipathic helices that insert into the lipid bilayer. All disease-associated single point mutations have been identified to be within these helical regions of α-synuclein: V15A, A30P, E46K, H50Q, G51D, A53T, and A53V. However, the effects of these mutations on the bound states of the two α helices of the protein have yet to be fully characterized. In this report, we use a tryptophan fluorescence assay to measure the binding of the α helices of these PD-associated mutants to lipid membranes within the lipid-depletion regime. We characterize the binding behavior of each helix, revealing that, generally, the PD-associated mutants shift the equilibrium bound state away from the N-terminal helix of the protein toward helix 2 at lower lipid concentrations. Altogether, our results indicate that disruption to the equilibrium binding of the two α helices of α-synuclein could play a role in PD progression.

SIGNIFICANCE Our work here identifies a uniform effect of Parkinson's disease-associated mutations (V15A, A30P, E46K, H50Q, G41D, A53T, A53V) on the equilibrium lipid-bound state of α-synuclein. Through the use of a lipid-depletion framework, we reveal a shift in the bound state toward helix 2 of the protein across all studied mutants, a state that may play a critical role within the α-synuclein fibrillization and aggregation pathways in disease progression. In addition to its biological implications within the α-synuclein field, our work highlights the importance of considering lipid depletion in studying protein:lipid binding, as using the appropriate depletion binding model can reveal critical system information.

INTRODUCTION

Parkinson's disease (PD) is a neurodegenerative disease, primarily characterized by a decline in motor and cognitive function (1). Although not deadly, PD progression results in severe impacts on quality of life with no existing cures or preventive treatments. The disease affects over half a million adults in the United States with onset at an average age of 62 years (2). However, early-onset PD has been observed in patients with genetic markers within the SNCA gene (3).

The SNCA gene codes for the protein α-synuclein, which has been directly linked to irregular protein aggregation and formation of toxic Lewy bodies (LBs) within neurons—a common marker of PD (4). Although α-synuclein's function within the neuron is not fully understood, it is known to bind to the lipid membranes of synaptic vesicles (SVs), where it is proposed to play a role in the trafficking of SVs and neurotransmitter release into the synaptic cleft (5). Dysregulation in protein/membrane binding can lead to lipid membrane-templated α-synuclein fibrillization (6) and has been proposed to result in LB formation (7,8), where the primary components of LBs are α-synuclein and other protein and lipid species found within the neuron and the membrane of SVs (7,9).

In the cytosol of the neuron, α-synuclein forms an intrinsically disordered protein (10). However, in the presence of lipid membranes, its N terminus (residues 1–95) forms an extended α-helical region that partially inserts into the membrane (11), whereas its C terminus (residues 96–140) remains disordered and forms the projecting domain. This lipid-binding region of α-synuclein can be treated as two α helices, where helix 1 roughly comprises residues ~1–37 and helix 2 of residues ~45–95 (Fig. 1 *a*) (12,13). Although these helices are separated by a region that remains disordered, the binding of each helix is still likely

Submitted October 13, 2023, and accepted for publication May 1, 2024.
*Correspondence: kayeelee@uchicago.edu
Editor: Antje Pokorny Almeida.
https://doi.org/10.1016/j.bpj.2024.05.002

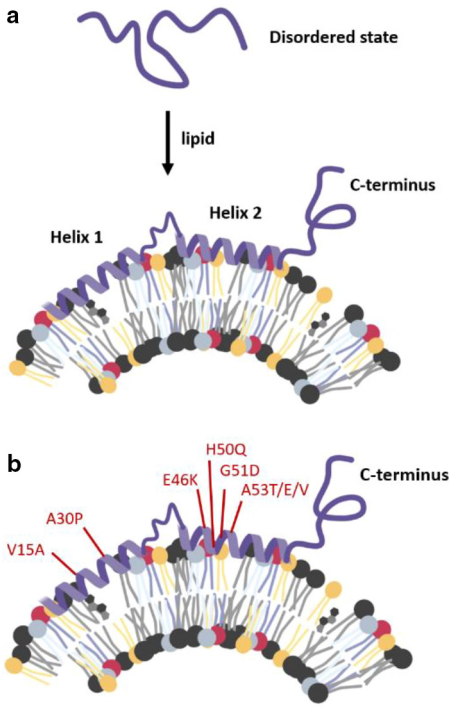

FIGURE 1 Location of PD-associated mutations in the lipid binding region of α-synuclein
(*a*) The transition of α-synuclein from an intrinsically disordered state to two α helices in the presence of a lipid membrane. (*b*) Location of PD-associated site mutations (*red*) within the lipid-binding region of α-synuclein. Figures are created with BioRender.com. To see this figure in color, go online.

dependent on the bound state of the other. The two helices are amphipathic (11), allowing residues to form hydrophobic contacts with lipid tails and hydrophilic contacts with the aqueous environment outside the synaptic vesicle. Positively charged residues interact with negatively charged lipid headgroups, further stabilizing the helices on the surface of the membrane (14). Of importance, all PD-associated genetic point mutations in SNCA are found within the lipid-binding region of α-synuclein: V15A, A30P, E46K, H50Q, G51D, A53T, and A53V (Fig. 1 *b*) (3).

Previous work has shown that fibrillization of α-synuclein may be membrane templated (15), with a few studies linking α-synuclein point mutations to an increased rate of fibril formation (16,17). However, the mutations do not appear to uniformly affect the lipid-binding properties of α-synuclein. For instance, the A30P mutant decreases α-synuclein's affinity for lipid membranes (18,19), whereas the E46K increases its affinity (19). Additionally, there are only limited datasets on how the mutations differentially affect each helix of the protein. As binding studies of α-synuclein are sensitive to experimental conditions, it is difficult to compare the effects of the mutations across studies. There is a need for a comprehensive, uniform analysis of how all the PD-associated point mutations affect interactions between α-synuclein and lipid membranes with helix-specific resolution.

We performed lipid titrations of the wild type (WT) and PD-associated variants of α-synuclein with an emphasis on the bound state of each helix using a tryptophan fluorescence assay. These binding curves were fitted to a lipid-depletion model (20), where the binding-site density served to directly evaluate the effect of PD-associated mutations on the binding behavior of the two helices. Our data reveal that PD-associated mutations uniformly shift the equilibrium bound state of the protein toward helix 2, a previously unidentified behavior of PD-associated variants and one that warrants further exploration to elucidate PD progression. Furthermore, our work demonstrates how the binding-site density of the lipid-depletion model can be used alongside measures of affinity to provide detail on protein binding behavior within the lipid-depletion model.

MATERIALS AND METHODS

Binding parameters within the depletion regime

The extended nature of its two helices requires α-synuclein to interact with a large surface area of the membrane. Although individual lipid species, such as phosphoserine (PS), may increase the affinity of α-synuclein for the membrane (21), many other membrane features that are not easily quantifiable, such as defects, are needed to accommodate the insertion of the full length of both α helices. A "binding site" for α-synuclein forms from any collection of lipid species that accommodates all the membrane parameters and lipid contacts that α-synuclein requires across the length of both α helices for the protein to fully associate with the membrane.

Previous research within the field has highlighted several key membrane parameters that affect α-synuclein's affinity for lipid membranes, including vesicle curvature and lipid tail/headgroup composition (21,22). No single parameter can solely characterize the binding of α-synuclein, as multiple configurations of lipid species can provide the necessary protein:lipid contacts. This results in a diversity of distinct lipid configurations that constitute binding sites for α-synuclein. Additionally, for α-synuclein to fully insert into the membrane, lipids must assemble or rearrange to locally contain the necessary lipid contacts and available surface space under the protein footprint. Therefore, although α-synuclein directly interacts with only a few dozen lipids within these binding sites, the protein requires many more lipids to indirectly support those interactions and these lipids are also depleted from the pool of available lipids.

In characterizing the α-synuclein:membrane system, we must first establish a suitable quantitative framework that reflects this rapid depletion of available lipid by α-synuclein (23). When the measured bound fraction of protein is dictated by the availability of the limited binding sites rather than the affinity of the protein for these sites, the protein is found to be within the lipid-depletion regime. Within this regime (i.e., high protein concentration with respect to lipid-binding sites), all available binding sites are occupied by proteins. As a result, the lipid available for binding $[L]_{free}$ can no longer be approximated to be equal to the total lipid concentration $[L]_{tot}$. Therefore, although the affinities for many protein:ligand systems can be adequately analyzed through the Michaelis-Menten binding equation (24), this general model cannot be directly applied to quantify the α-synuclein:membrane interactions investigated in the depletion regime. Instead, the explicit, mathematical dependence of the bound fraction of protein (f_{bound}) can be quantified through a depletion model with fit parameters of σ and K_d, where $[P]_{tot}$ and $[L]_{tot}$ are the total protein and lipid concentrations, respectively (Eq. 1) (23).

$$f_{bound} = \frac{1}{2[P]_{tot}}\left(\sigma \times K_d + [P]_{tot} + \sigma \times [L]_{tot} - \left(\left(\sigma \times K_d + [P]_{tot} + \sigma \times [L]_{tot}\right)^2 - 4[P]_{tot}\sigma \times [L]_{tot}\right)^{\frac{1}{2}}\right) \quad (1)$$

Here, the σ parameter is the binding-site density which, in brief, is the lipid density at which the membrane parameters required for a single protein to bind are present. For example, a σ value of 0.01 would indicate that on average a binding site that accommodates all the required protein:lipid contacts is available over 100 lipid molecules across both leaflets of the lipid bilayer. Importantly, this value does not indicate that α-synuclein directly interacts will all the lipids; instead, it represents the density of available binding sites on the membrane. Within this binding equation, the K_d is the effective dissociation constant *per lipid* and is a measure of the average affinity of the protein for a lipid in its binding site. Of note, within Eq. 1, the K_d is multiplied by σ, so the effective $K_{d,\,eff}$, given by $K_{d,\,eff} = K_d \times \sigma$, would represent the affinity of the protein for all the lipids required to assemble to form a binding site. The use of Eq. 1 and interpretation of these parameters is relevant for when the protein:membrane binding is in the depletion regime, when the protein concentration is greater than the product of σ and K_d ($[P]_{tot} > \sigma \times K_d$).

Traditionally, protein:ligand binding is analyzed through the K_d, but, within the depletion regime, the binding at lower lipid concentrations is dictated by the σ parameter. This mathematical dependence is illustrated by the approximation of Eq. 1 using $(\sigma \times K_d/[P]_{tot}) << 1$ (Eqs. 2, 3 and 4).

$$f_{bound} = \frac{1}{2} + \frac{\sigma \times K_d}{2[P]_{tot}} + \frac{\sigma \times [L]_{tot}}{2P_{tot}} - \frac{1}{2}\left(\left(\frac{\sigma \times K_d}{P_{tot}} + 1 + \sigma \times \frac{[L]_{tot}}{P_{tot}}\right)^2 - 4\sigma \times \frac{1}{P_{tot}} \times [L]_{tot}\right)^{\frac{1}{2}}\right) \quad (2)$$

$$f_{bound} \cong \frac{1}{2} + \frac{\sigma \times [L]_{tot}}{2P_{tot}} - \frac{1}{2}\left(\left(1 + \sigma \times \frac{[L]_{tot}}{P_{tot}}\right)^2 - 4\sigma \times \frac{1}{P_{tot}} \times [L]_{tot}\right)^{\frac{1}{2}}\right) \quad (3)$$

$$f_{bound} \cong \frac{\sigma \times [L]_{tot}}{P_{tot}} \quad (4)$$

At these lower lipid concentrations, the binding curve can be approximated by a line with a slope proportional to σ (Fig. 2 *a*). As shown, even a $[P]_{tot}/\sigma \times K_d$ ratio as low as ~3 (green curve in Fig. 2 *a*) results in the binding curve that can be well approximated at lower lipid concentrations by a line with a slope equal to $\sigma/[P]_{tot}$. It is important to note that, within the depletion regime, the K_d primarily describes protein behavior corresponding to the region between the curve's linear region and the plateau (25). As a result, the binding-site density, σ, is a more reliable and descriptive parameter of binding than the K_d under limited lipid availability

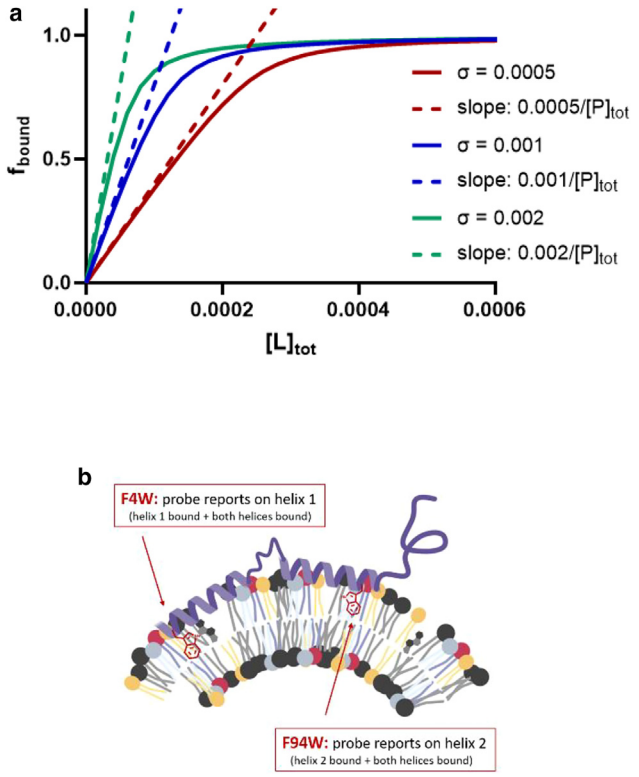

FIGURE 2 Model binding within the depletion regime (*a*) Modeled binding curves (*solid lines*) for Eq. 1 at varying binding-site densities $\sigma = 0.0005$ (*red*), $\sigma = 0.001$ (*blue*), and $\sigma = 0.002$ (*green*) at constant $[P]_{tot} = 125$ nM, and $K_d = 20$ μM, corresponding to a $[P]_{tot}/(\sigma \times K_d)$ ratio of 12.5, 6.25, and 3.125, respectively. Dashed lines corresponding to a slope of $\sigma/[P]_{tot}$ for each curve are shown to demonstrate the region corresponding to the lipid-depletion regime at lower lipid concentrations. (*b*) Location of helix 1 reporter (F4W) and helix 2 reporter (F94W). To see this figure in color, go online.

and should be used to analyze protein binding behavior at lower lipid concentrations.

Many in vitro lipid-binding assays of α-synuclein, such as NMR, CD, and tryptophan fluorescence spectroscopy, are done at high protein concentrations. In combination with the protein's high affinity for the membrane, these assays are therefore confined to the lipid-depletion regime, evident by the observed rapid linear increase in bound fraction across α-synuclein's binding curves (26). This regime may also be physiologically relevant, as local concentrations of α-synuclein within the synapse can reach ~22 μM, (27) and the surface area of SVs has a high density of other proteins (60% occupancy by mass (28)), which contribute to the depletion of the membrane parameters that α-synuclein requires to bind. Although we fitted our α-synuclein:lipid-binding curves using both σ and K_d, our analysis focuses on the σ parameter, as the binding-site density holds critical information about the experimental and physiological binding behavior of the protein under limited lipid availability.

Within our work, the binding-site density, σ, can be used to investigate how PD-associated mutations alter binding-site availability for the two helices of α-synuclein. These mutations likely alter the identity of binding sites, as changes to the structure of the protein may require a separate collection of membrane parameters to accommodate its insertion. For example, the E46K mutation within α-synuclein may alter its lipid charge preferences, whereas the A53V mutation may alter preferences for membrane fluidity or curvature. Although the binding of α-synuclein is often treated as binary, the interactions of α-synuclein and the membrane

comprise a collection of states in which the two helices are engaged with the membrane to varying extents, and it is likely that these mutations may differentially affect the binding-site density of the two helices of the protein. The binding-site density cannot provide lipid-specific information, but it can probe how mutations alter the global lipid environment's ability to accommodate local regions of the protein. This allows for a comparison of the behavior of different proteins across identical membrane conditions. Furthermore, within the lipid-depletion regime, the binding-site density of each helix's bound state is critical as it dictates the distribution of these states on the membrane surface.

To measure the lipid binding of α-synuclein with helix-specific resolution, we introduced two minimally invasive mutations at sites F4W and F94W for the use of tryptophan fluorescence spectroscopy, a technique that can robustly quantify local interactions of α-synuclein with lipid membranes (29). Tryptophan is a naturally fluorescent amino acid with an emission spectrum that is sensitive to its environment. In comparison to an aqueous environment, the emission spectrum of tryptophan in a hydrophobic environment is blue shifted and higher in intensity, and thus this technique can monitor local tryptophan insertion into the hydrophobic environment of a lipid membrane. To individually probe at the bound state of each of the two helices in α-synuclein, we chose to label at the F4W and F94W sites, located at the front and tail edges of helix 1 and helix 2, respectively (Fig. 2 *b*); from here on these are referred to as helix 1 reporter and helix 2 reporter.

The reporters, given their locations, only report on membrane binding when these ends of the helices are engaged with the membrane. Pfefferkorn et al. have previously validated that neither of these mutations affects the protein's overall affinity for the membrane (30). α-Synuclein that includes reporters at both sites (dual reporter) would serve as a readout for any membrane-bound state where at least one tryptophan site is engaged. Through these reporters, we can investigate the effect of each PD-associated variant on the effective binding-site density for each of the helices in α-synuclein.

α-Synuclein protein and mutant purification

N-terminal acetylated WT α-synuclein and associated mutants were expressed/purified as previously described with a few modifications (31). In short, the sequence for WT α-synuclein was encoded into a pET-21a backbone from which all mutants were generated using site-directed mutagenesis. The pET-21a plasmids were then transformed into BL21 cells that have been pretransformed with the pNatB plasmid that encodes for the N-α-acetyltransferase. From a starter culture of 25 mL, the BL21 cells were grown at 37°C under ampicillin and chloramphenicol resistance. At a density corresponding to optical density 600 = 0.6, protein expression was induced with 1 μM isopropyl β-D-1-thiogalactopyranoside for 4 h at 37°C. Cells were then pelleted at 7000 g for 15 min and resolubilized in buffer A (20 mM Tris-HCl, pH 8.0, 5 mM EDTA, 1 mM PMSF, pinch of DNAase). Cells were lysed by sonication for 10 min, after which the pH was adjusted to 3.5 with NaOH. Cell debris was pelleted by centrifugation at 18,000 × *g* for 15 min. The supernatant containing the N-acetylated α-synuclein was adjusted to pH 7.0 with HCl. Ammonium sulfate was added to 50% saturation, and the protein was spun at 4°C for 1 h. The final precipitate containing the protein was isolated as a pellet through centrifugation at 18,000 × *g* for 30 min. The pellet was resuspended in 3 mL of water, and the protein was dialyzed overnight at 4°C into deionized water using 0.5- to 3-mL capacity, 3.5k MWCO Slide-A-Lyzer Dialysis Cassettes. Finally, the dialyzed protein was injected onto a Superdex 200 10/300 column (GE Healthcare Lifesciences) and eluted at ∼15 mL with HEPES-buffered saline buffer (10 mM HEPES pH 7.2, 150 mM NaCl, 0.1% azide). Fractions containing the protein were pooled, aliquoted, flash-frozen with liquid nitrogen, and stored at −80°C until use. Protein concentration was measured using a NanoDrop (Thermo Fisher Scientific) with predicted absorbances of $A_{280} = 11{,}460\ M^{-1}cm^{-1}$ and $A_{280} = 16{,}960\ M^{-1}cm^{-1}$ for single (either F4W or F94W) and double (both F4W and F94W) tryptophan mutants, respectively. Of note, protein preparations containing mutations at the A53 site (A53E, A53T, and A53V) tend to aggregate during dialysis, resulting in significantly reduced protein yields. However, the final protein purified off the Superdex 200 was in monomeric form, as determined by elution volume and SDS-PAGE. Before use, tryptophan fluorescence spectra of the thawed protein were taken to monitor the state of the protein and detect possible protein aggregations (see Figs. S2 and S3 for discussion of the A53E mutant).

Lipid preparations

1,2-Dioleoyl-sn-glycero-3-phosphocholine (DOPC), 1,2-dioleoyl-sn-glycero-3-phospho-L-serine (sodium salt) (DOPS), 1,2-dioleoyl-sn-glycero-3-phosphoethanolamine (DOPE), and cholesterol (CHOL, ovine wool) were purchased in powder form from Avanti Polar Lipids (Alabaster, AL, USA). The Lipex Extuder was purchased from Evonik Transferra Nanosciences (Burnaby, BC, Canada). Small unilamellar vesicles (SUVs) were prepared as previously described (32). In short, lipids were suspended in high-pressure liquid chromatography-grade chloroform as 18 mM stock solutions. Lipids were aliquoted into a preweighed vial in the desired ratio of 55:20:15:10 DOPC:DOPS:DOPE:CHOL, and the chloroform was then evaporated under a nitrogen stream. The vials were incubated overnight in a desiccator under a vacuum. The lipid mixtures were then rehydrated in filtered HEPES-buffered saline buffer (10 mM HEPES, 150 mM NaCl, pH 7.2) to a lipid concentration of 18 mM. The lipid mixtures were shaken at 37°C for 40 min to form multilamellar vesicles. These vesicles were then subjected to seven freeze-thaw cycles using a dry-ice-ethanol bath and a 40°C water bath. Next, the vesicles were passed once through a membrane with 200-nm pore size (Whitman Nucleophore membrane; 25 mm in diameter) under 100 psi of ultrahigh-purity argon gas and then passed 15 times through membranes with 50-nm pore size under 400-psi argon. Final SUV size and polydispersity were measured to be ∼70 nm by dynamic light scattering (Zen3600 Malven Nano Zetasizer, Malvern, UK).

Tryptophan shift binding assay

The tryptophan fluorescence binding assay was performed on all mutants as previously described (32) at 125 nM protein and lipid ranges of 0–2500 μM. All tryptophan fluorescence data were collected at 37°C on a Fluorolog-3 spectrophotometer (Horiba, Kyoto, Japan) in 10-mm pathlength Quartz cuvettes (Starna Cells, Atascadero, CA) with a USHIO Xenon short arc lamp. Samples were excited with 280-nm light and emission was measured from 300 to 420 nm (slit width of 2 nm). A spectrum that serves as a standard (to account for lipid scattering) for each lipid concentration was collected before the addition of protein. Before scanning, samples containing protein were stirred for 1.5 min, which was verified to be sufficient for binding to equilibrate at various lipid concentrations. At least three samples were collected for each lipid concentration with measurements generally aligning. Of note, this method is highly sensitive to temperature, vesicle composition, and protein stability; it is therefore important to ensure that handling of samples is uniform across all protein and lipid samples.

Tryptophan fluorescence data were analyzed through custom MATLAB code (32). For each lipid concentration examined, $S_{measured}$ was fit to a bound fraction f_{bound} using a linear combination of spectra corresponding to the tryptophan in solution S_{sln} and bound state S_{bound} (Eq. 5). The solution state was measured at a lipid concentration of 0 μM, whereas the lipid concentration corresponding to the bound state (as indicated by overlapping spectra with increasing lipid) varied among the mutants but was generally ∼1000 μM.

$$S_{measured} = f_{bound} \times S_{bound} + (1 - f_{bound}) \times S_{sln} \quad (5)$$

The binding curves generated from each lipid titration were fitted using a lipid-depletion model to characterize the binding of the mutants (20).

RESULTS

We first characterized the binding of the two helices of WT α-synuclein to SUVs with a lipid composition of 55:20:15:10 DOPC:DOPS:DOPE:CHOL using the tryptophan fluorescence assay. To independently probe at each helix, we used both the helix 1 reporter (F4W mutant) and the helix 2 reporter (F94W mutant). The binding curves for the two reporters were each fitted to a lipid-depletion model (Eq. 1) with fit parameters of the dissociation constant, K_d, and the binding-site density, σ, described above.

The binding curves for helix 1 reporter and helix 2 reporter are shown in Fig. 3 *a* and *b*, respectively, and their corresponding site density σ values, obtained from fitting the curves to Eq. 1, were found to be $\sigma_{H1} = 0.00113 \pm 0.00006$ and $\sigma_{H2} = 0.00110 \pm 0.00021$ in units of inverse lipids. Converting to units of lipids, we see that a binding site that accommodates a single helix occurs on average every 909 lipids across the bilayer. Furthermore, fitting resulted in dissociation constant values for helix 1 and helix 2 reporters of $K_{d,\ H1} = 23.9 \pm 3.62$ μM and $K_{d,\ H2} = 16.5 \pm 8.49$ μM, respectively. Within the error of one another, this suggests that the helices have approximately similar affinities for the lipids directly involved in the binding site. Overall, binding curves for the helix 1 reporter and helix 2 reporter alone suggest that the membrane contains similar binding-site densities for the two helices of WT α-synuclein and that the two helices have similar affinities for the lipids involved in the binding.

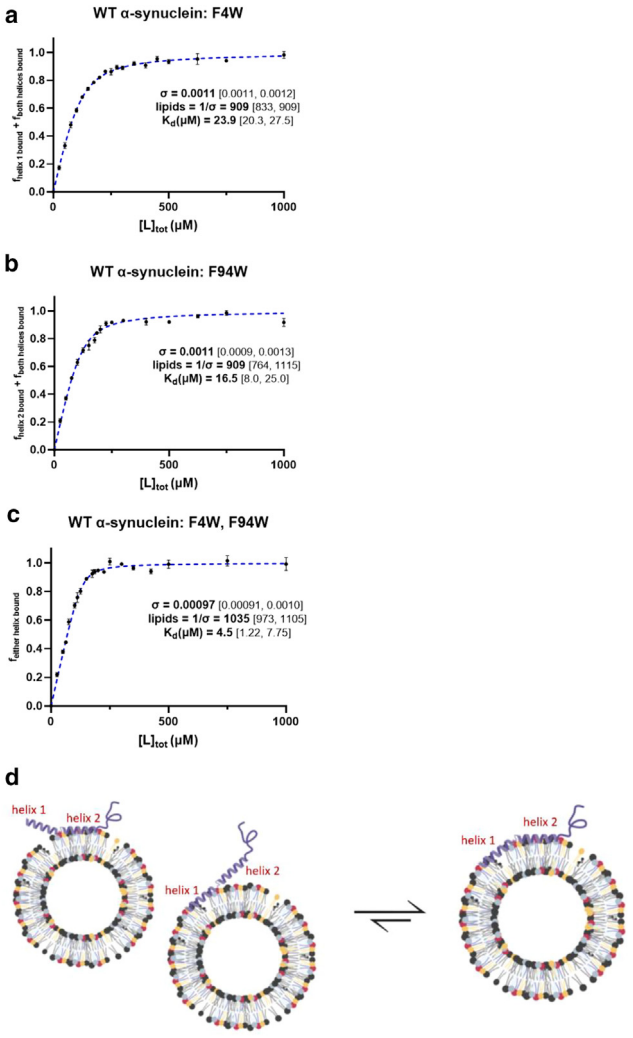

FIGURE 3 Lipid-binding data of WT α-synuclein
Binding curve of WT α-synuclein at 125 nM protein concentration, using (*a*) helix 1 reporter, (*b*) helix 2 reporter, and (*c*) dual reporter. The best fit obtained using Eq. 1 is shown as a dashed line for each curve. Error bars represent standard deviation. Parameter fits are shown with a 95% confidence interval. (*d*) Cartoon depiction of equilibrium in bound states of α-synuclein. To see this figure in color, go online.

We next performed the same lipid titration of WT α-synuclein with the dual reporter, where σ_D and $K_{d,DR}$ were fitted to 0.0009 ± 0.000062 1/lipids and 4.5 ± 3.3 μM, respectively (Fig. 3 *c*). The similar σ values of the single- vs. dual-reporter systems (Fig. S1) indicate that the two helices of WT α-synuclein seek out similar membrane parameters in binding, suggesting that the bound state involves both helices interacting with the membrane. Altogether, these data show that the equilibrium bound state of WT α-synuclein leans toward having both helices engaged with the membrane within the lipid-depletion regime (Fig. 3 *d*).

This reporter system was then extended to examine how PD-associated mutants differentially affect the binding of the two helices of α-synuclein. As a case study, we generated α-synuclein with the PD-associated mutation E46K containing either the singular helix 1 or helix 2 reporter and performed the tryptophan fluorescence assay to generate binding curves. The fitted σ values for helix 1 reporter (E46K) and helix 2 reporter (E46K) were $\sigma_{H1} = 0.00083 \pm 0.00006$ and $\sigma_{H2} = 0.0018 \pm 0.00021$ in units of inverse lipids, reflecting a binding site for the helices every 1198 and 556 lipids across the bilayer, respectively (Fig. 4 *a* and *b*). We can further compare WT and E46K results by examining the linear region of the bound fraction for each reporter (Fig. 4 *c*). We can see that a binding site that accommodates helix 2 of E46K is more abundant on the membrane than for helix 1—a difference that does not exist for WT α-synuclein. Although previous studies have suggested that the E46K mutation increases the binding of α-synuclein for lipid membranes (19,26), our results here suggest that this may be a property largely conferred on the protein by increased binding-site availability for helix 2 on the membrane. Altogether, our findings from the reporter systems suggest that the E46K mutation within α-synuclein shifts the equilibrium toward helix 2 within the lipid-depletion regime (Fig. 4 *d*), and the lipid membrane contains fewer binding sites that accommodate the insertion of helix 1 in comparison to helix 2. These results are further supported by the binding curve for E46K α-synuclein with the dual reporter, where the slope of the binding

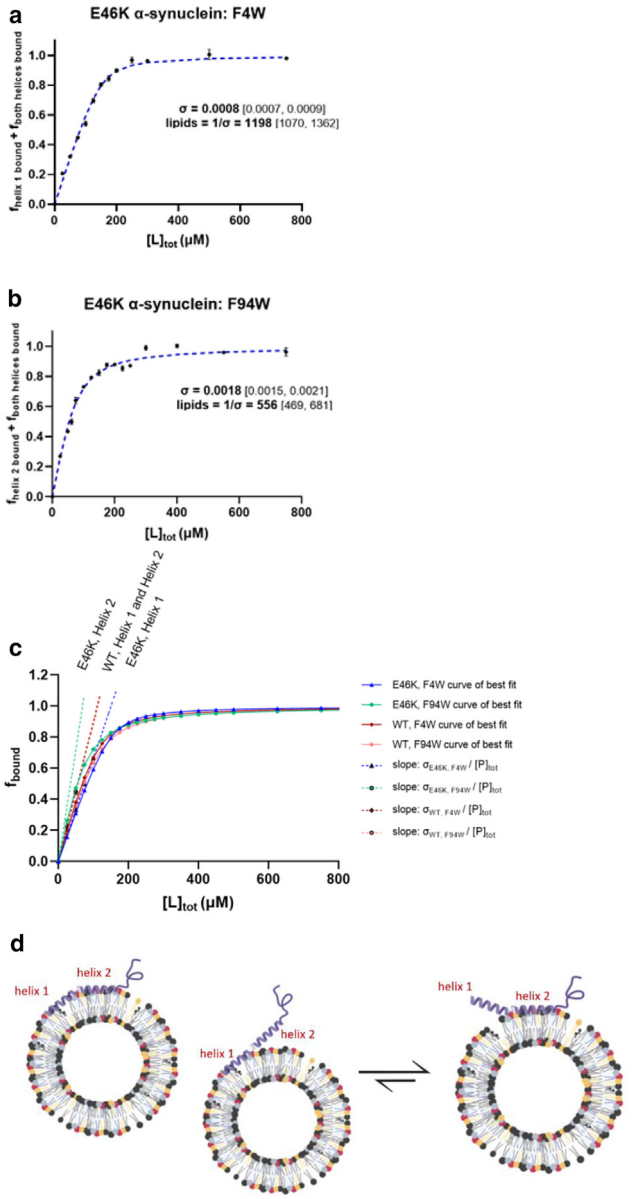

FIGURE 4 Lipid-binding data of the E46K mutant of α-synuclein
Binding curve of E46K α-synuclein at 125 nM protein, using (*a*) helix 1 reporter and (*b*) helix 2 reporter. Best-fit curves using Eq. 1 are shown as dashed lines. Error bars represent standard deviation. Parameter fits are shown with a 95% confidence interval. (*c*) Best-fit curves of WT and E46K α-synuclein for helix 1 and helix 2 reporters (*solid lines*). Dashed lines corresponding to $\sigma[P]_{tot}$ for each of the curves, using the σ parameter fit from Eq. 1, are shown to highlight the difference in binding-site density in the E46K (*green and blue*) mutant in comparison to the WT (*red and pink*). (*d*) Cartoon depiction of equilibrium in bound states of E46K α-synuclein. Of note, in comparison to WT, a state in which only helix 2 is bound in a more dominant state for E46K than for WT α-synuclein. To see this figure in color, go online.

curve of E46K in the depletion regime is closer to that of the helix 1 reporter (Fig. S1), demonstrating the dependence of the binding of the entire protein on the helix with lower binding-site availability.

A similar analysis was performed on six more PD-associated mutants: V15A, A30P, H50Q, G51D, A53T, and A53V (Fig. 5 *a*.). The fit parameters from the binding curves for the three reporter systems are summarized in Table 1, whereas Fig. 5 *b* displays the number of lipids that constitutes a binding site for WT and all PD-associated mutants examined ($1/\sigma$). Across all seven PD-associated mutants, we see that a higher binding-site density (lower $1/\sigma$) for helix 2 than for helix 1 alone, or for both helices. We performed an F-test on the WT and each PD-associated mutant of α-synuclein comparing each fit to that in which σ is constrained to be the same for both helix reporters. Although WT α-synuclein exhibits no difference in the fit between the helix 1 and helix 2 reporter binding curves, the PD-associated mutants all showed a statistically significant ($p < 0.05$) difference between σ fits for the two reporters, with σ for the helix 1 reporter being consistently lower (Table 2). Of note, the parameter fits of the A30P, H50Q, G51D, and A53T mutant curves are not statistically significant under the application of the Bonferroni correction ($p < 0.00625$). Altogether, these results indicate that the helices of α-synuclein are not equally sensitive to PD-associated mutations, resulting in a shift in the equilibrium bound state of the protein toward helix 2.

DISCUSSION

Although PD-associated mutations are not required for the development and progression of PD, these mutations do accelerate the onset and severity of associated symptoms (3). In studying PD-associated mutants, we can gain insights into the potential neurotoxicity of WT α-synuclein. The true bound state of α-synuclein comprises a distribution of states in which the two helices of α-synuclein are bound to the membrane to varying extents; identifying which states are related to the dysfunction of α-synuclein is critical to uncovering the role α-synuclein binding to membranes plays within PD. In comparison to WT α-synuclein, a unifying feature of these PD-associated mutations emerges: across all seven mutants studied, there is a shift in the equilibrium bound states of α-synuclein toward helix 2. This conserved equilibrium shift emphasizes that relative binding-site availability between the two helices may play an important role in PD progression.

The tryptophan fluorescence assay used serves as a powerful tool to probe site-specific interactions between the α helices of the protein and the lipid membrane. It allows us to quantitively characterize the effects of the PD-associated mutants on the bound state of each of the helices. Furthermore, the lipid-depletion model employed here relates the binding of the protein to binding-site availability, allowing for the binding-site density, σ, to 1) reflect relevant membrane parameters and solution conditions for binding, and 2) directly gauge the relative propensity of the two helices for membrane binding across the PD-associated

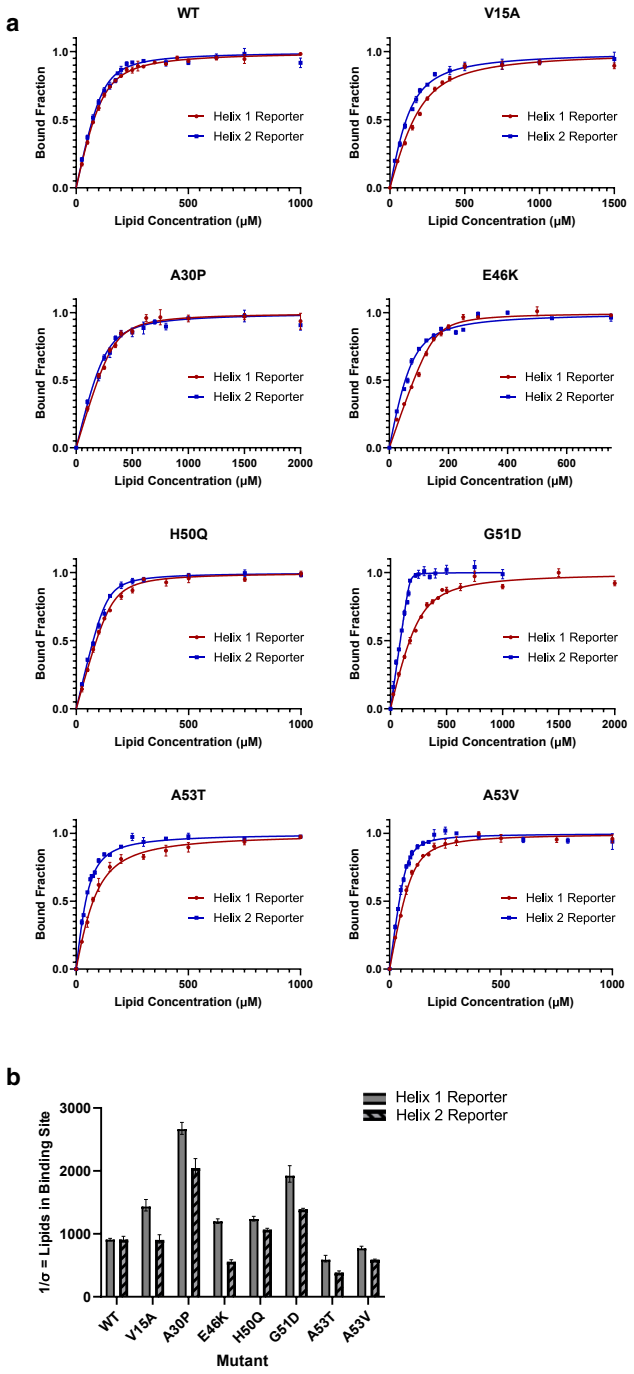

FIGURE 5 Lipid-binding data of PD-associated α-synuclein mutants (*a*) Binding curves from the helix 1 and helix 2 reporters for WT and PD-associated mutants. Binding curves were fitted to Eq. 1. Error bars represent standard deviation. (*b*) The inverse of the binding-site density ($1/\sigma$) is shown for the WT and each of the seven PD-associated mutants of α-synuclein. Data for each sample were fitted to Eq. 1 independently for helix 1 and helix 2. Error bars represent 95% condifence intervals. Of note, parameter fits for all PD-associated mutants show a statistically significant difference between the helix 1 and helix 2 reporter ($p < 0.05$); see Table 2. To see this figure in color, go online.

mutants. Of note, the specific locations of the helix 1 reporter and helix 2 reporter allow this assay to only probe for bound states in which the front and back ends of helix 1 and helix 2, respectively, are engaged with the membranes. Any partially bound state in which these residues are not inserted into the membrane will therefore be considered an unbound state within the analysis.

In comparison to a binary association model, the in-depth analysis of the two α helices through an equilibrium model between states in which a single helix or both helices are bound reveals important features of PD-associated mutations. Our results indicate that all PD-associated mutations shift the equilibrium toward a bound helix 2 state due to higher binding-site availability for helix 2 over helix 1. Importantly, our results highlight how an appropriate binding model for quantifying protein:membrane interactions can reveal critical system information that may otherwise be obscured. Analyzing the lipid-binding behavior of α-synuclein through a framework that incorporates the σ parameter may be useful in relating other features of α-synuclein to binding-site availability on the membrane. For example, the two α helices of α-synuclein have been proposed to adopt either a horseshoe or extended state, depending on sample conditions (33,34). It is likely that these states require a separate set of lipid contacts, resulting in a difference in the binding-site density for the two helices. Future work may help uncover the relationship between specific lipid membrane parameters and the binding-site availability for the two conformations.

The findings of this study may address some of the inconsistent results within the α-synuclein mutant literature. For example, some previous studies have reported increased lipid binding for the E46K mutant (19), whereas others (26) have shown negligible attenuation of binding. Our results here (increased binding-site availability for helix 2, along with a mild decrease for helix 1) suggest that the method used in quantifying α-synuclein binding could significantly influence the binding data obtained. In the case of the E46K mutant, a method that reports on any bound state of α-synuclein (e.g., fluorescence microscopy (19)) would see an overall increase in lipid binding, whereas methods that more directly probe the bound state of the helices (e.g., nuclear magnetic resonance or circular dichroism (26)) may measure little change (26) or a slight decrease in membrane association of the E46K mutant compared to WT. Our work thus underscores the importance of considering the distribution of bound states of α-synuclein in uncovering the effects of mutations and membrane parameters on the binding behavior of α-synuclein and its role within PD. It is worth noting that, although we cannot know the true ratio of protein to available lipid within the neuron, the depletion regime may be physiologically relevant for α-synuclein binding due to high neuronal α-synuclein concentrations and the crowded environment of the lipid membranes of SVs. Interestingly, the mutant with the largest difference in the binding of the two helices, G51D, is associated with much earlier onset and more severe symptoms in PD progression (3).

TABLE 1 1/σ and K_d values for the WT and PD-associated α-Synuclein mutants

Mutant	Lipids = 1/σ from helix 1 reporter fit	Lipids = 1/σ from helix 2 reporter fit	K_d from helix 1 reporter fit (μM)	K_d from helix 2 reporter fit (μM)
WT	909 [972, 1105]	909 [833, 909]	23.8 [20.2, 27.5]	16.5 [8.0, 25.0]
V15A	1433 [1158, 1879]	903 [714, 1227]	69.0 [28.8, 109.2]	52.8 [31.2, 74.6]
A30P	2663 [2341, 3086]	2045 [1671, 2635]	27.5 [5.2, 49.7]	37.9 [12.8, 63.1]
E46K	1198 [1070, 1362]	556 [470, 681]	7.8 [1.1, 14.5]	19.3 [11.4, 27.1]
H50Q	1236 [1107, 1399]	1066 [991, 1154]	12.2 [3.6, 20.8]	8.6 [5.1, 12.2]
G51D	1923 [1526, 2551]	1388 [1323, 1458]	51.8 [15.7, 87.9]	1.1 [0.2, 2.4]
A53T	588 [455, 862]	384 [309, 488]	38.3 [21.1, 55.6]	18.9 [13.9, 24.1]
A53V	769 [699, 909]	588 [543, 633]	15.0 [8.7, 21.3]	7.0 [4.5, 9.5]

Binding curves from each reporter were fitted to Eq. 1. Values in table are displayed with 95% confidence intervals.

The α-synuclein field has established that the initial residues of the N terminus are essential for triggering the α helix formation and the subsequent binding of the protein (12). Meanwhile, residues 61–95, termed the non-amyloid component (NAC) domain, have been proposed to have reduced lipid association and increased propensity to aggregate (35). Our results here point to a possibly larger role played by helix 2 in stabilizing α-synuclein at the membrane than previously thought. As the position of the helix 2 reporter is at residue 94, any measured bound state for helix 2 would require the engagement of its end with the membrane. Similarly, a measured bound state for helix 1 reporter (located at residue 4) would require the beginning of helix 1 to engage with the membrane. Therefore, the decrease in binding of helix 1 over helix 2 across the PD-associated mutants indicates that, although helix 1 may be critical in triggering binding of WT α-synuclein, helix 2 plays a more dominant role over helix 1 in associating the protein with the membrane for the PD-associated mutants.

The uniformity of the equilibrium shift observed across all PD-associated mutants suggests that a state in which the helix 2 is more tightly bound is related to the dysfunction of α-synuclein within PD, possibly through membrane disruption or lipid-templated aggregation as several studies have identified the importance of solution-exposure of the N terminus of α-synuclein in promoting fibrillization (36,37). Although this work does not extend to uncovering how this state promotes aggregation, plausible mechanisms include 1) the solution-exposed first α helix acting as a nucleation site, 2) helix 2 acting as a nucleation site for membrane-templated aggregation, and 3) the shifted equilibrium alters binding partners of α-synuclein. Interestingly, Bell et al. find that a conserved feature across five acetylated PD-associated variants of α-synuclein is the ability of their lipid-induced aggregates to seed fibril elongation from the monomer form (38). This feature separates the five studied PD-associated variants from WT α-synuclein, warranting future exploration into how the binding of the two α helices of α-synuclein alter the specific structural properties of the aggregates to allow for elongation. It would be additionally of interest to examine whether variants with the other PD-associated mutations studied within our work, V15A and A53V, similarly allow for fibril elongation. Importantly, this difference between WT and the PD-associated variants was only conserved across the acetylated versions of the proteins where non-acetylated A30P and E46K were unable to induce fibril elongation from their respective monomer forms (38). As the protein used within our work is also acetylated, it would be prudent to study the binding curves of the α helices of non-acetylated A30P and E46K to further solidify the correlation between these features of α-synuclein.

Our findings reveal a uniform effect of PD-associated mutants on the binding of α-synuclein to lipid membranes. We highlight the utility of using an appropriate binding model in quantifying α-synuclein's binding to membranes with limited binding-site availability—a lipid-depletion regime that is often accessed within α-synuclein-binding studies due to the protein's interactions with a large set of lipid parameters. Altogether, our work suggests that a lipid-bound state in which helix 2 of α-synuclein is more tightly bound may play a critical role within PD progression and warrants future exploration for its role in protein aggregation and dysregulation.

TABLE 2 F-test results for each Reporter pair across WT and each PD-associated mutant

Mutant	F-test statistic for helix 1 vs. helix 2 reporter	*p* value for helix 1 vs. helix 2 reporter
WT	0.0002935	0.9864
V15A	9.51	0.0052
A30P	6.101	0.0214
E46K	50.08	<0.0001
H50Q	6.053	0.0218
G51D	8.117	0.0078
A53T	5.023	0.0338
A53V	26.55	<0.0001

SUPPORTING MATERIAL

Supporting material can be found online at https://doi.org/10.1016/j.bpj.2024.05.002.

AUTHOR CONTRIBUTIONS

S.M. and K.Y.C.L. designed research. S.M. performed research. S.M. and D.K. analyzed data. S.M., M.T., and D.K. contributed to tool development. E.J.A. discussed results. S.M. and K.Y.C.L. wrote the paper.

ACKNOWLEDGMENTS

We thank Dr. Elena Solomaha for her expertise in the instrumentation used in this study and Dr. Peter Chung for his expertise in the protein purification methods used.

We thank Dr. Tim Bartels for his generous gift of the WT α-synuclein plasmid used in this study.

The work was supported by the National Science Foundation through MCB-1950525 (to K.Y.C.L.). K.Y.C.L. acknowledges support from The University of Chicago Materials Research Science and Engineering Center (NSF/DMR- 2011854) and The University of Chicago Biophysics Core Facility. Additional National Institutes of Health support was provided under grant no. R01 AI155984 (to E.J.A.).

DECLARATION OF INTERESTS

The authors declare no competing interests.

REFERENCES

1. Armstrong, M. J., and M. S. Okun. 2020. Diagnosis and Treatment of Parkinson Disease. *JAMA.* 323:548–560.
2. Pagano, G., N. Ferrara, …, N. Pavese. 2016. Age at onset and Parkinson disease phenotype. *Neurology.* 86:1400–1407.
3. Whittaker, H. T., Y. Qui, …, H. Houlden. 2017. Multiple system atrophy: genetic risks and alpha-synuclein mutations. *F1000Res.* 6:2072.
4. Siddiqui, I. J., N. Pervaiz, and A. A. Abbasi. 2016. The Parkinson Disease gene SNCA: Evolutionary and structural insights with pathological implication. *Sci. Rep.* 6, 24475.
5. Gao, V., J. A. Briano, …, J. Burré. 2023. Functional and Pathological Effects of α-Synuclein on Synaptic SNARE Complexes. *J. Mol. Biol.* 435, 167714.
6. Mori, A., Y. Imai, and N. Hattori. 2020. Lipids: Key Players That Modulate α-Synuclein Toxicity and Neurodegeneration in Parkinson's Disease. *Int. J. Mol. Sci.* 21:3301.
7. Mahul-Mellier, A.-L., J. Burtscher, …, H. A. Lashuel. 2020. The process of Lewy body formation, rather than simply α-synuclein fibrillization, is one of the major drivers of neurodegeneration. *Proc. Natl. Acad. Sci. USA.* 117:4971–4982.
8. Choi, Y. R., S. J. Park, and S. M. Park. 2021. Molecular events underlying the cell-to-cell transmission of α-synuclein. *FEBS J.* 288:6593–6602.
9. McCormack, A., D. J. Keating, …, T. Chataway. 2019. Abundance of Synaptic Vesicle-Related Proteins in Alpha-Synuclein-Containing Protein Inclusions Suggests a Targeted Formation Mechanism. *Neurotox. Res.* 35:883–897.
10. Meade, R. M., D. P. Fairlie, and J. M. Mason. 2019. Alpha-synuclein structure and Parkinson's disease – lessons and emerging principles. *Mol. Neurodegener.* 14:29.
11. Jao, C. C., B. G. Hegde, …, R. Langen. 2008. Structure of membrane-bound alpha-synuclein from site-directed spin labeling and computational refinement. *Proc. Natl. Acad. Sci. USA.* 105:19666–19671.
12. Bartels, T., L. S. Ahlstrom, …, K. Beyer. 2010. The N-Terminus of the Intrinsically Disordered Protein α-Synuclein Triggers Membrane Binding and Helix Folding. *Biophys. J.* 99:2116–2124.
13. Kaur, U., and J. C. Lee. 2020. Unroofing site-specific α-synuclein–lipid interactions at the plasma membrane. *Proc. Natl. Acad. Sci. USA.* 117:18977–18983.
14. Jao, C. C., A. Der-Sarkissian, …, R. Langen. 2004. Structure of membrane-bound α-synuclein studied by site-directed spin labeling. *Proc. Natl. Acad. Sci. USA.* 101:8331–8336.
15. Lee, H.-J., C. Choi, and S.-J. Lee. 2002. Membrane-bound α-Synuclein Has a High Aggregation Propensity and the Ability to Seed the Aggregation of the Cytosolic Form. *J. Biol. Chem.* 277:671–678.
16. Ohgita, T., N. Namba, …, H. Saito. 2022. Mechanisms of enhanced aggregation and fibril formation of Parkinson's disease-related variants of α-synuclein. *Sci. Rep.* 12:6770.
17. Lima, V. d. A., L. A. do Nascimento, …, C. Follmer. 2019. Role of Parkinson's Disease-Linked Mutations and N-Terminal Acetylation on the Oligomerization of α-Synuclein Induced by 3,4-Dihydroxyphenylacetaldehyde. *ACS Chem. Neurosci.* 10:690–703.
18. Ysselstein, D., M. Joshi, …, J.-C. Rochet. 2015. Effects of impaired membrane interactions on α-synuclein aggregation and neurotoxicity. *Neurobiol. Dis.* 79:150–163.
19. Stöckl, M., P. Fischer, …, A. Herrmann. 2008. α-Synuclein Selectively Binds to Anionic Phospholipids Embedded in Liquid-Disordered Domains. *J. Mol. Biol.* 375:1394–1404.
20. Kerr, D., T. Suwatthee, …, K. Y. C. Lee. 2024. BINDING EQUATIONS FOR THE LIPID COMPOSITION DEPENDENCE OF PERIPHERAL MEMBRANE-BINDING PROTEINS. *Biophys. J.* 123:885–900.
21. Sarchione, A., A. Marchand, …, M.-C. Chartier-Harlin. 2021. Alpha-Synuclein and Lipids: The Elephant in the Room? *Cells.* 10:2452.
22. Middleton, E. R., and E. Rhoades. 2010. Effects of Curvature and Composition on α-Synuclein Binding to Lipid Vesicles. *Biophys. J.* 99:2279–2288.
23. Kerr, D., T. Suwatthee, …, K. Y. C. Lee. 2024. Binding equations for the lipid composition dependence of peripheral membrane-binding proteins. *Biophys. J.* 123:885–900.
24. Srinivasan, B. 2022. A guide to the Michaelis–Menten equation: steady state and beyond. *FEBS J.* 289:6086–6098.
25. Jarmoskaite, I., I. AlSadhan, …, D. Herschlag. 2020. How to measure and evaluate binding affinities. *Elife.* 9, e57264.
26. Rovere, M., A. E. Powers, …, T. Bartels. 2019. E46K-like α-synuclein mutants increase lipid interactions and disrupt membrane selectivity. *J. Biol. Chem.* 294:9799–9812.
27. Afitska, K., A. Fucikova, …, D. A. Yushchenko. 2019. α-Synuclein aggregation at low concentrations. *Biochim. Biophys. Acta, Proteins Proteomics.* 1867:701–709.
28. Poudel, K. R., and J. Bai. 2014. Synaptic vesicle morphology: a case of protein sorting? *Curr. Opin. Cell Biol.* 26:28–33.
29. Kraft, C. A., J. L. Garrido, …, G. Romero. 2009. Quantitative Analysis of Protein-Lipid Interactions Using Tryptophan Fluorescence. *Sci. Signal.* 2:pl4.
30. Pfefferkorn, C. M., and J. C. Lee. 2010. Tryptophan Probes at the α-Synuclein and Membrane Interface. *J. Phys. Chem. B.* 114:4615–4622.
31. Chung, P. J., Q. Zhang, …, K. Y. C. Lee. 2019. α-Synuclein Sterically Stabilizes Spherical Nanoparticle-Supported Lipid Bilayers. *ACS Appl. Bio Mater.* 2:1413–1419.
32. Kerr, D., Z. Gong, …, K. Y. C. Lee. 2021. How Tim proteins differentially exploit membrane features to attain robust target sensitivity. *Biophys. J.* 120:4891–4902.
33. Ferreon, A. C. M., Y. Gambin, …, A. A. Deniz. 2009. Interplay of α-synuclein binding and conformational switching probed by

single-molecule fluorescence. *Proc. Natl. Acad. Sci. USA.* 106:5645–5650.

34. Georgieva, E. R., T. F. Ramlall, …, D. Eliezer. 2010. The Lipid-binding Domain of Wild Type and Mutant α-Synuclein. *J. Biol. Chem.* 285:28261–28274.

35. Doherty, C. P. A., S. M. Ulamec, …, D. J. Brockwell. 2020. A short motif in the N-terminal region of α-synuclein is critical for both aggregation and function. *Nat. Struct. Mol. Biol.* 27:249–259.

36. McGlinchey, R. P., X. Ni, …, J. C. Lee. 2021. The N terminus of α-synuclein dictates fibril formation. *Proc. Natl. Acad. Sci. USA.* 118.

37. Stephens, A. D., M. Zacharopoulou, …, G. S. K. Schierle. 2020. Extent of N-terminus exposure of monomeric alpha-synuclein determines its aggregation propensity. *Nat. Commun.* 11:2820.

38. Bell, R., M. Castellana-Cruz, …, M. Vendruscolo. 2023. Effects of N-terminal Acetylation on the Aggregation of Disease-related α-synuclein Variants. *J. Mol. Biol.* 435, 167825.